Miscibility and Hydrogen Bonding in Blends of Poly(vinylphenol- co -methyl methacrylate) with Poly(ethylene oxide)

2 **AUTHORS**, INCLUDING:

Shiao-Wei Kuo

National Sun Yat-sen University

267 PUBLICATIONS **5,591** CITATIONS

Miscibility and Hydrogen Bonding in Blends of Poly(vinylphenol-*co*-methyl methacrylate) with Poly(ethylene oxide)

Shiao Wei Kuo and Feng Chih Chang*

Institute of Applied Chemistry, National Chiao Tung University, Hsin Chu, Taiwan, Republic of China

Received January 9, 2001; Revised Manuscript Received March 1, 2001

ABSTRACT: Blends of poly(vinylphenol-*co*-methyl methacrylate) (PVPh-*co*-PMMA) with poly(ethylene oxide) (PEO) were prepared by solution casting from tetrahydrofuran (THF) solution. The miscibility behavior and hydrogen bonding of blends were investigated by differential scanning calorimetry (DSC), Fourier transform infrared spectroscopy (FTIR), and solid-state nuclear magnetic resonance (NMR). Experimental results indicate that PEO was miscible with PVPh-*co*-PMMA as shown by the existence of single composition-dependent glass transition temperatures over the entire composition range by DSC. In addition, a negative polymer−polymer interaction energy density "*B*" was calculated based on the melting depression of PEO using the Nishi−Wang equation. Solid-state NMR reveals single-exponential decay of proton spin−lattice relaxation times in the rotating frame ($T_{1\rho}{}^{H}$) in the amorphous PVPh-*co*-PMMA phase. Furthermore, FTIR and solid-state NMR results reveal that at least three competing equilibria are present in the blend; self-association of PVPh-*co*-PMMA copolymer (hydroxyl−hydroxyl and hydroxyl−carbonyl) and hydroxyl−ether interassociation between PVPh and PEO. Quantitative results show that although the hydroxyl−ether interassociation is favored at room temperature, the hydroxyl−carbonyl self-association dominates at higher temperatures (>70 °C). The Painter−Coleman association model (PCAM) can predict three interacting functional groups based on our experimental results at various temperatures.

Introduction

The miscibility of polymer blends has received much attention in polymer science. Some of this research has been performed with blends in which one or two components are semicrystalline. A common component in crystalline miscible blends is a polyether, poly-(ethylene oxide) (PEO), a highly crystalline polymer miscible with several amorphous polymers through hydrogen bonding.[1−3] Various techniques have been adopted to determine the miscibility of polymer blends, including thermal analysis,[4] dynamic mechanical analysis,[5] small-angle X-ray scattering,[6] microscopy[7] and solid-state NMR.[8−13] Furthermore, DSC can determine whether one or two T_g values and a single T_g point is the most conventionally used criterion for the miscibility of a polymer blend. On the contrary, an immsicible polymer blend exhibits more than one T_g. A single compositionally dependent glass transition indicates full miscibility with a dimension on the order of 20−40 nm. Over the years, various equations have been offered to predict the variation of the glass transition temperature of random copolymers or miscible blends as a function of composition, which can be well interpreted in terms of specific interaction within a polymer blend.

By Fourier transform infrared (FTIR) spectroscopy, the carbonyl, hydroxyl, and ether vibrations have been proved to be excellent clues to detect the molecular interaction.[14−17] Solid state ^{13}C NMR is also a highly effective means of studying the miscibility and hydrogen bonding of polymer blends. The ^{13}C chemical shift and line shape in cross-polarization and magic angle spinning (CP/MAS) spectra can identify chemical environments of carbon in the blend, since the chemical shift and the line shape are highly sensitive to the local electron density. If a specific interaction affects the local electron density, a change in chemical shift can be observed. This approach has been widely offered as evidence of the interaction between the blend components. The scale of miscibility of a polymer blend can be estimated from proton spin−lattice relaxation times in the rotating frame ($T_{1\rho}{}^{H}$), measured by solid-state NMR.

In addition to studying the miscibility of PVPh-*co*-PMMA with PEO blends by DSC and solid-state NMR, this study provides evidence of specific intermolecular association and self-association by using FTIR and solid-state NMR. The fraction of hydrogen bonding of the carbonyl group in the PVPh-*co*-PMMA/PEO blend is also calculated at various temperatures, as compared with the inter and self-association equilibrium constants of the Painter−Coleman association model[18] (PCAM). Experimental data are obtained using the PCAM results to predict successfully the fraction carbonyl group that are hydrogen bonded.

Experiment

Samples. The polymers used in this study, poly(vinylphenol-*co*-methyl methacrylate) (PVPh-*co*-PMMA) with VPh contents of 51 mol %, and poly(ethylene oxide) (PEO) with M_n = 20 000 were obtained from Aldrich Co. Figure 1 illustrates the chemical structures of (PVPh-*co*-PMMA) and PEO.

Blend Preparations. Blends of various (PVPh-*co*-PMMA)/ PEO compositions were prepared by solution casting. Tetrahydrofuran solutions containing a 5 wt % polymer mixture were stirred for 6−8 h and cast on a Teflon dish. The solution was allowed to evaporate slowly at room temperature for 1 day. The blend films were then dried at 50 °C for 2 days.

Characterizations. Differential Scanning Calorimetry. T_gs of blend films were determined by a DSC with a Du-Pont (DSC-9000), with a scan rate of 20 °C/min over a temperature range of 30−150 °C. The measurement was made using a 5−10 mg sample on a DSC sample cell after the sample

* To whom corresponding should be addressed. E-mail: changfc@cc.nctu.edu.tw. Telephone: 886-3-5712121 ext. 56502. Fax: 886-3-5723764.
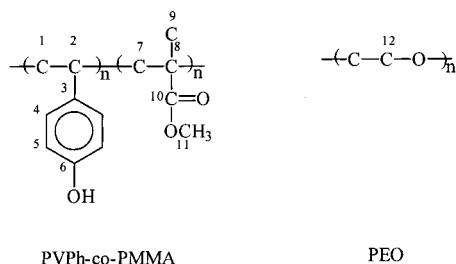
Figure 1. Chemical structures of PVPh-*co*-PMMA and PEO and their atom numbering schemes

was quickly cooled to −100 °C from the melt of the first scan. The glass transition temperature is taken as the midpoint of the heat capacity transition between the upper and lower points of deviation from the extrapolated liquid and glass lines. The isothermal crystallization from the melt was also examined by DSC. The samples were melted at 80 °C for 10 min, cooled quickly to the crystallization temperature (T_c), and then maintained at T_c for 12 h. After isothermal crystallization was complete, the samples were cooled at 0 °C and heated to 100 °C at a rate of 10 °C/min to measure the melting temperature (T_m).

Infrared Spectroscopy. Infrared spectra of polymer blend films were determined by using the conventional NaCl dish method. The THF solution containing the blend was cast onto a NaCl disk and dried under conditions similar to those used in the bulk preparation. The film used in this study was thin enough to obey the Beer−Lambert law. FTIR measurements were recorded on a Nicolet Avatar 320 FT-IR spectrophotometer, and 32 scans were collected with a spectral resolution of 1 cm⁻¹. Owing to that fact that the sample containing hydroxyl groups is water sensitive, a pure nitrogen flow was used to purge the IR optical box in order to maintain dry sample films. IR spectra recorded at elevated temperatures were obtained by using a cell mounted inside the temperature-controlled compartment of the spectrometer.

Solid State NMR. High-resolution solid state ¹³C NMR experiments were carried out at room temperature using a Bruker DSX-400 spectrometer operating at resonance frequencies of 399.53 and 100.47 MHz for ¹H and ¹³C, respectively. The ¹³C CP/MAS spectra were measured with a 3.9 μs 90° pulse, with 3 s pulse delay time, acquisition time of 30 ms, and 2048 scans were accumulated. All NMR spectra were taken at 300 K using broad band proton decoupling and a normal cross-polarization pulse sequence. A magic angle sample spinning (MAS) rate of 5.4 kHz was used to eliminate resonance broadening due to the anisotropy of chemical shift tensors. The proton spin−lattice relaxation time in the rotating frame ($T_{1\rho}^H$) was measured indirectly via carbon observation using a 90°-τ-spin lock pulse sequence prior to cross-polarization. The data acquisition was performed via ¹H decoupling and delay time (τ) ranging from 0.3 to 15 ms with a contact time of 1.0 ms.

Results and Discussion

Thermal Analyses. Differential scanning calorimetry (DSC) is extensively used to investigate miscibility in polymer blends. A single compositionally dependent glass transition is an indication of full miscibility at a dimensional scale between 20 and 40 nm. Single T_g behavior represents macroscopically and implies full miscibility of the blend. Figure 2 shows DSC analyses of the PVPh-*co*-PMMA/PEO blends of various compositions. The pure amorphous PVPh-*co*-PMMA exhibits one T_g at 134.9 °C while the T_gs of PVPh-*co*-PMMA shift to lower temperatures as the PEO content in the blend increases. Furthermore, the melting temperature of the PEO component in the blend decreases with the increase of the PVPh-*co*-PMMA content. Table 1 summarizes the thermal properties of PVPh-*co*-PMMA,
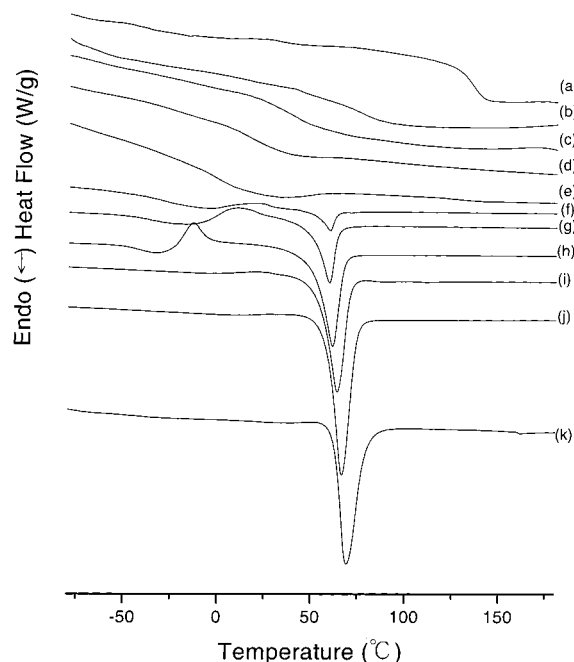

Figure 2. DSC scans of PVPh-*co*-PMMA/PEO blends with different compositions: (a) 100/0; (b) 90/10; (c) 80/20; (d) 70/30; (e) 60/40; (f) 50/50; (g) 40/60; (h) 30/70; (i) 20/80; (j) 10/90; (k) 0/100.

Table 1. Thermal Properties of PVPh-*co*-PMMA/PEO Blends

PVPh-*co*-PMMA/PEO	T_g (°C)	T_m (°C)	ΔH_f (J/g)	T_c (°C)	ΔH_c (J/g)
100/0	134.9				
90/10	71.9				
80/20	42.2				
70/30	18.3				
60/40	2.7				
50/50	−19.6	59.0	5.6	20.0	−4.2
40/60	−32.7	59.0	44.7	10.5	−30.4
30/70	−43.3	60.9	84.9	−13.8	−31.9
20/80	−32.9	63.6	104.0		
10/90	−38.2	66.3	128.6		
0/100	−67.0	69.2	175.7		

PEO, and their blends. All PVPh-*co*-PMMA/PEO blends show only a single glass transition temperature (T_g) over the entire blend composition. A single T_g strongly suggests that these are fully miscible blends with a homogeneous amorphous phase.

Various equations have been offered to predict the variation of the glass transition temperature of a random copolymer or miscible blend as a function of composition. The dependence of T_g on the composition of the miscible PVPh-*co*-PMMA/PEO blends is shown in Figure 3. The experimental T_g vs composition curve is not well fit either with the Fox[19] or the Gordon−Taylor equation.[20] However, the Kwei equation[21] fits the experimental data well. The Kwei equation is as follows

$$T_g = \frac{W_1 T_{g1} + k W_2 T_{g2}}{W_1 + k W_2} + q W_1 W_2 \qquad (1)$$

where W_1 and W_2 denote weight fractions of the compositions, T_{g1} and T_{g2} represent the corresponding blend component glass transition temperatures, and k and q are fitting constants. $k = 4$ and $q = 32$ are obtained from the nonlinear least-squares "best fit" values. Here q is a parameter corresponding to the strength of hydrogen
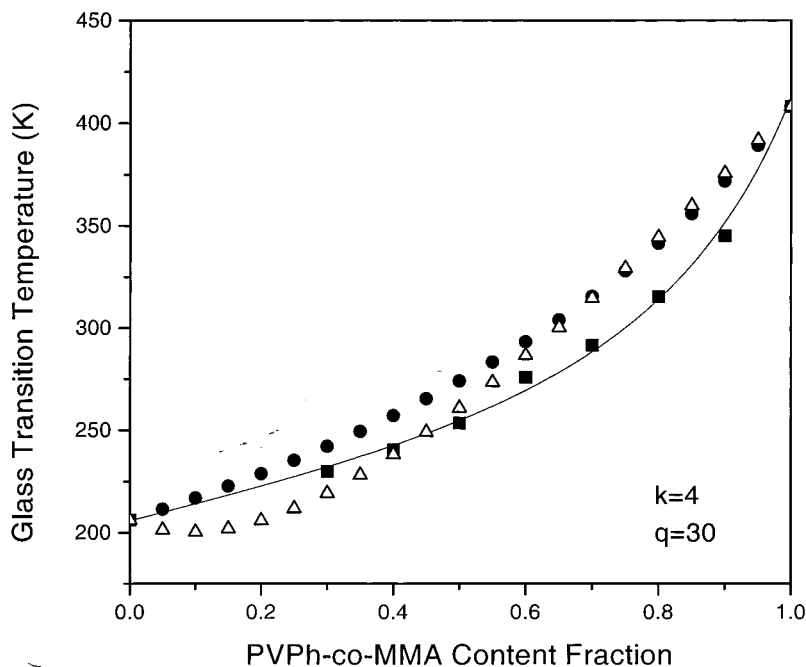
Figure 3. T_g vs composition curves based on (■) experimental data, (●) the Fox equation, (△) the Gordon–Taylor equation, and (–) the Kwei equation.

bonding in the blend, which should be considered as a balance between the breaking of the self-association hydrogen bonding and the forming of the interassociation. The value of q depends on the change of entropy corresponding to the change in the number of hydrogen bonding interactions with the PEO in this blend. In this study, a positive q of 30 was obtained, indicating a strong intermolecular interaction between PEO and PVPh-*co*-PMMA.

Equilibrium Melting Temperature and Melting Point Depression. The depression of the melting point of a crystalline polymer blended with an amorphous polymer provides important information about its miscibility and its associated polymer–polymer interaction parameter. The temperature reduction is caused by morphological effects and for thermodynamic reasons. From the thermodynamic consideration, thermodynamic properties of the crystalline component in the amorphous phase can be determined. When two polymers are miscible in the molten state, the chemical potential of the crystallizable polymer is decreased due to the addition of the second component. This fact leads to a reduction in the equilibrium melting temperature of the resulting blend. The data obtained in this study were analyzed by the Nishi–Wang equation[22] based on the Flory–Huggins theory.[23] The melting point depression is given by eq 2,[22,23] where T_m^0 and $T_{m_2}^0$ denote the

$$\frac{1}{T_m^0} - \frac{1}{T_{m_2}^0} = \frac{-R}{\Delta H_{2u}} \frac{V_{2u}}{V_{1u}} \left[\frac{\ln \phi_2}{x_2} + \left(\frac{1}{x_2} - \frac{1}{x_1} \right)(1 - \phi_2) + \chi_{12}(1 - \phi_2)^2 \right] \quad (2)$$

equilibrium melting points of the pure crystallizable component and of the blend, respectively. V_{2u} and V_{1u} are the molar volumes of the repeating units of the polymers. R is the universal gas constant. ΔH_{2u} is the heat of fusion of the perfectly crystallizable polymer per mole of repeat unit; subscript 1 represents the amorphous polymer, and subscript 2 the crystalline polymer.

x_1 and x_2 are degrees of polymerization; Φ is the volume fraction of the component in the blend, and χ_{12} is the polymer–polymer interaction parameter. When both x_1 and x_2 are large, for high molecular weight polymers, these related terms in eq 2 can be neglected. The interaction parameter χ_{12} can be written as

$$\chi_{12} = \frac{BV_{1u}}{RT} \quad (3)$$

Substituting eq 3 into eq 2 yields the Nishi–Wang equation[22]

$$T_m^0 - T_{m_2}^0 = -T_m^0 \frac{BV_{2u}}{\Delta H_{2u}} \phi_1^2 \quad (4)$$

where $\Delta H_{2u}/V_{2u}$ is the latent heat of fusion of 100% crystalline component per unit volume and B denotes the interaction energy density between blend components.

The method of Hoffman and Weeks[24] has been used to determine the equilibrium melting temperatures for pure PEO (T_m^0) and blends ($T_{m_2}^0$) of given compositions, to eliminate the morphological effect from the melting point depression. Figure 4 presents the Hoffman–Weeks plots to obtain the equilibrium melting points for pure PEO and various PVPh-*co*-PMMA/PEO blends. The $T_{m_2}^0$ values decrease with increasing PVPh-*co*-PMMA content. An immiscible or partially miscible blend typically does not show the depression of the equilibrium melting point (T_m^0), $T_{m_2}^0$ is depressed significantly with increasing the content of the amorphous polymer for a miscible blend, especially one containing specific interaction between the components. As also shown in Figure 4, the melting point depression, ΔT_m, for PVPh-*co*-PMMA/PEO blends increases linearly with the volume fraction of the amorphous component (Φ_1). The weight fraction is converted into the volume fraction using the molar volume of monomeric units determined by a group contribution method.[18] A B value of −29.23 is calculated from the slope of Figure 5
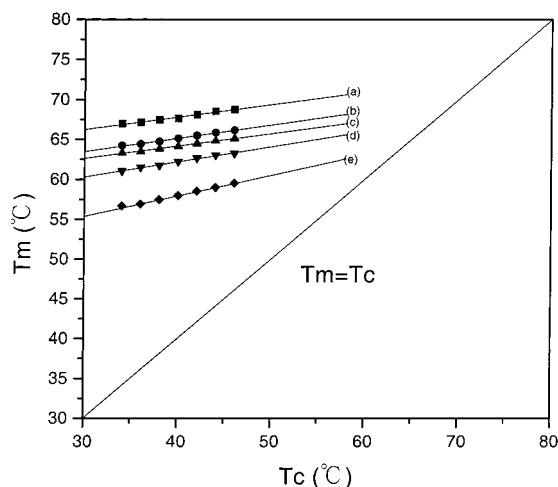
Figure 4. Hoffman–Weeks plots for PVPh-*co*-PMMA/PEO blends: (a) 0/100; (b) 10/90; (c) 20/80; (d) 30/70; (e) 40/60.
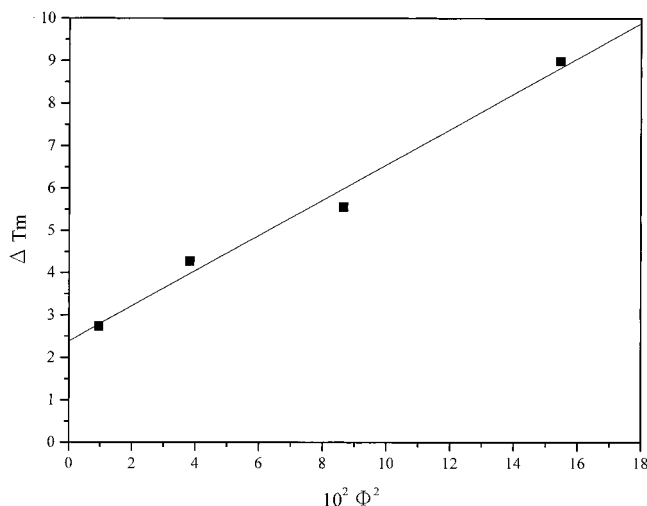

Figure 5. Plots of the equilibrium melting temperature depression vs the square of the volume of fraction of PVPh-*co*-PMMA.

according to eq 4 and the data of $V_{2u} = 38.1$ cm^3/mol and $\Delta H_{2u} = 1980$ cal/mol.[25] The negative B value is consistent with a miscible system. According to eq 4, the intercept of a plot of ΔT_m vs Φ_1^2 should be close to zero. However, the line has a finite intercept because of the significant entropic effect of blending two polymers.

Fourier Transform Infrared Spectroscopy Analyses. Infrared spectroscopy has been proven a highly effective means of investigating specific interactions between polymers. This tool can be used to study the mechanism of interpolymer miscibility through the formation of hydrogen bonding both qualitatively and quantitatively. Self-association may occur especially by hydroxyl–hydroxyl and hydroxyl–carbonyl hydrogen bonding, taking into account the chemical structure of PVPh-*co*-PMMA. Figure 6 shows the infrared spectra of the carbonyl stretching measured at 25 °C ranging from 1660 to 1800 cm^{-1} for PVPh-*co*-PMMA, PEO, and their blends. The carbonyl stretching for the pure PVPh-*co*-PMMA is split into two bands, absorption by free and hydrogen-bonded carbonyl groups at 1730 and 1705 cm^{-1}, respectively. These bands can be readily decomposed into two Gaussian peaks, with areas corresponding to the free carbonyl (1730 cm^{-1}) and the hydrogen-
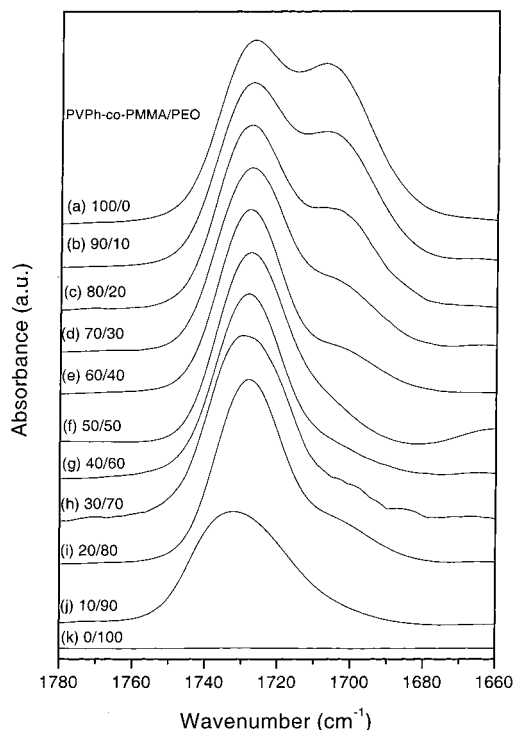

Figure 6. FTIR spectra recorded at room temperature in the 1660–1780 cm^{-1} region for PVPh-*co*-PMMA/PEO blends: (a) 100/0; (b) 90/10; (c) 80/20; (d) 70/30; (e) 60/40; (f) 50/50; (g) 40/60; (h) 30/70; (i) 20/50; (j) 10/90; (k) 0/100.

Table 2. Curve-Fitting Results of the PVPh-*co*-PMMA/PEO Blends at Room Temperature

blend (wt %)	free C=O			H-bonded C=O			fb
	ν (cm^{-1})	$W_{1/2}$ (cm^{-1})	A_f (%)	ν (cm^{-1})	$W_{1/2}$ (cm^{-1})	A_b (%)	(%)
100/0	1729.6	17.17	41.40	1706.3	24.24	58.60	48.55
90/10	1729.3	17.26	46.74	1705.7	24.45	53.26	43.17
80/20	1728.9	17.23	53.86	1704.8	23.06	46.14	36.35
70/30	1728.7	17.53	61.73	1706.3	26.56	38.27	29.24
60/40	1728.4	17.14	70.26	1704.5	23.79	29.74	22.00
50/50	1728.7	16.23	75.26	1712.7	18.53	24.74	17.97
40/60	1728.5	17.65	78.46	1709.8	17.94	21.54	15.47
30/70	1730.0	19.34	81.56	1710.3	18.00	19.44	13.09
20/80	1730.5	84.51	75.99	1709.7	23.07	15.01	10.53
10/90	1733.9	20.61	87.46	1717.0	24.11	12.54	8.73

*fb: fraction of hydrogen bonding

bonded carbonyl (1705 cm^{-1}) absorptions. Using the respective absorptivity coefficients allows us to calculate the fraction of these two carbonyl groups from the relative intensities of these two bands. The fraction of the hydrogen-bonded carbonyl group[18] is calculated from eq 5, where A_b and A_f are the peak areas corresponding

$$f_b^{C=O} = \frac{A_b/1.5}{A_b/1.5 + A_f} \quad (5)$$

to the hydrogen-bonded carbonyl and the free carbonyl groups, respectively. The conversion coefficient of 1.5 is the absorptivity ratio of these two bands, the "free" and "hydrogen-bonded" carbonyl groups, in an ester group.[18] Table 2 summarizes the curve fitting results indicating that the fraction of hydrogen bonded carbonyl groups decreases as PEO content increases. As a result, the PMMA carbonyl competes with the ether oxygen of PEO to form a hydrogen bond with the hydroxyl group of the PVPh. According to the Painter–Coleman as-

Table 3. Summary of the Self-Association and Interassociation Equilibrium Constants of PVPh-*co*-PMMA/PEO Blends

	equilib const K (25 °C)	enthalpy, ΔH (kcal/mol)
self-association[a]		
dimer formation K_2	21.0	−5.60
multimer formation K_B	66.8	−5.20
between VPh and MMA K_c	67.4	−4.20
interassociation between[b] PVPh and PEO	88.3	−5.40

polymer	molar vol (mL/mol)	mol wt (g/mol)	solubility param (cal/mL)$^{0.5}$	deg of polymn, DP
PVPh[c]	100.00	120.10	10.60	500
PMMA[c]	84.90	100.12	9.10	500
PEO[c]	38.10	44.06	9.40	500

[a] Reference 36. [b] Reference 37. [c] Estimated by using a group contribution method proposed by Coleman et al.[18]
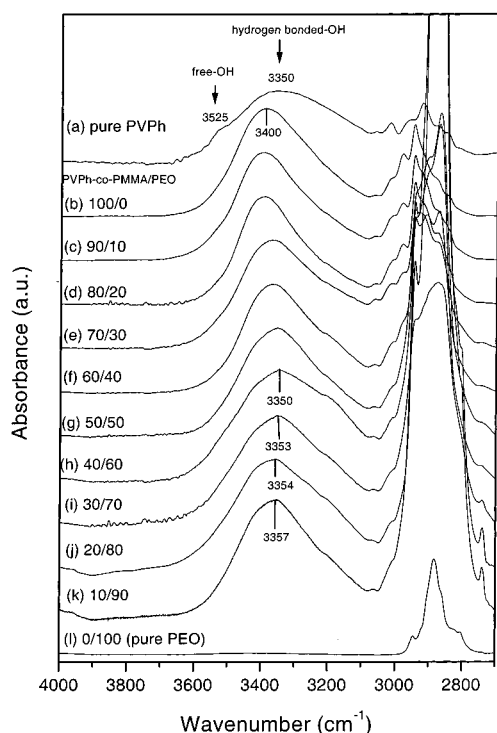

Figure 7. FTIR spectra recorded at room temperature in the 2700−4000 cm^{-1} region for pure PVPh and various PVPh-*co*-PMMA/PEO blends: (a) pure PVPh; (b) 100/0; (c) 90/10; (d) 80/20; (e) 70/30; (f) 60/40; (g) 50/50; (h) 40/60; (i) 30/70; (j) 20/50; (k) 10/90; (l) 0/100.

sociation model (PCAM), Table 2 shows that the decrease in the fraction of hydrogen bonded carbonyl groups with increasing PEO content implies that the interassociation equilibrium constant of hydroxyl−ether has a larger value than the self-associations equilibrium constant of hydroxyl−carbonyl at room temperature. Table 3 lists all the parameters required by the Painter−Coleman association model to estimate thermodynamic properties for the PVPh-*co*-PMMA/PEO blend.

Figure 7 shows the absorption region of the pure PVPh, PVPh-*co*-PMMA, and various PVPh-*co*-PMMA/PEO blends between 2700 and 4000 cm^{-1} at room temperature. As shown in Figure 7a, the pure PVPh polymer exhibits two bands in the hydroxy stretching region of the infrared spectrum. The free hydroxyl group
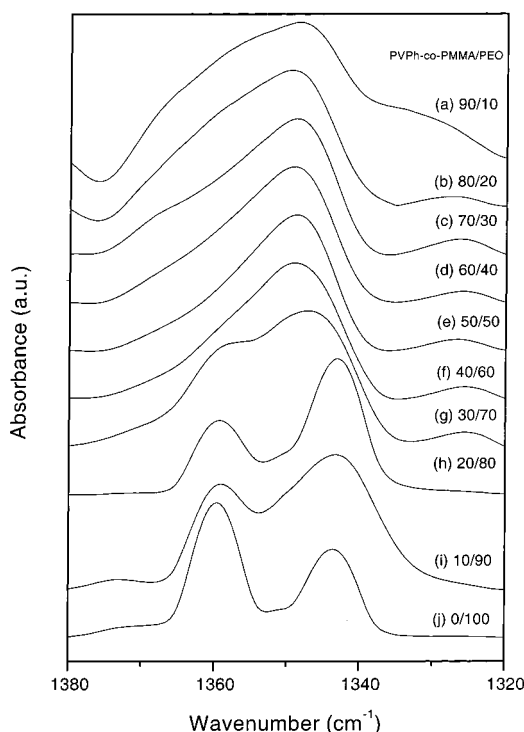

Figure 8. FTIR spectra recorded at room temperature at 1320 cm^{-1}-1380 cm^{-1} region for PVPh-*co*-PMMA/PEO blends: (a) 90/10; (b) 80/20; (c) 70/30; (d) 60/40; (e) 50/50; (f) 40/60; (g) 30/70; (h) 20/50; (i) 10/90; (j) 0/100.

absorption is located at 3525 cm^{-1}, while the hydrogen-bonded hydroxyl gives a broad absorption at 3350 cm^{-1} due to wide distribution of hydrogen-bonded hydroxyl groups. However, the pure PVPh-*co*-PMMA (Figure 7b) shows only one band at about 3400 cm^{-1} in the hydroxyl-stretching region of the infrared spectrum. This reflects the new distribution of hydrogen bonded between hydroxyl−hydroxyl and hydroxyl−carbonyl specific interactions. Furthermore, the band at 3400 cm^{-1} is shifted to 3350 cm^{-1}, a lower wavenumber, for blends containing 60 wt % PEO content (Figure 7g). This change is come from the switch from the intramolecular hydroxyl−carbonyl bond to the intermolecular hydroxyl−ether bond, indicating that there is hydrogen-bonding interaction between the PEO ether group and the hydroxyl group of PVPh. The average strength of the intermolecular interaction can be obtained by the extent of frequency difference ($\Delta \nu$) between the hydrogen bonded hydroxyl absorption and free hydroxyl absorption. A $\Delta \nu = 175$ cm^{-1} value for PVPh-*co*-PMMA/PEO = 40/60 is obtained which is stronger than that of the self-associated between hydroxyl and carbonyl of the pure PVPh-*co*-PMMA copolymer ($\Delta \nu = 125$ cm^{-1}), and this result is consistent with the positive q value obtained in the Kwei equation and the observed carbonyl stretching in the infrared spectra.

The CH$_2$ wagging region of the pure PEO and its blends with PVPh-*co*-PMMA is now examined. Figure 8 shows infrared spectra in the 1320−1380 cm^{-1} region of the pure PEO, and various PVPh-*co*-PMMA/PEO blends. As shown in Figure 8j, the bands at 1360 and 1343 cm^{-1} represent the crystalline phase of PEO.[26] These bands decrease slightly as the PVPh-*co*-PMMA content increases. The crystalline bands disappear at the PVPh-*co*-PMMA/PEO = 40/60 blend and are replaced by a broad band roughly centered at 1350 cm^{-1} corresponding to the amorphous phase. The PEO crys-
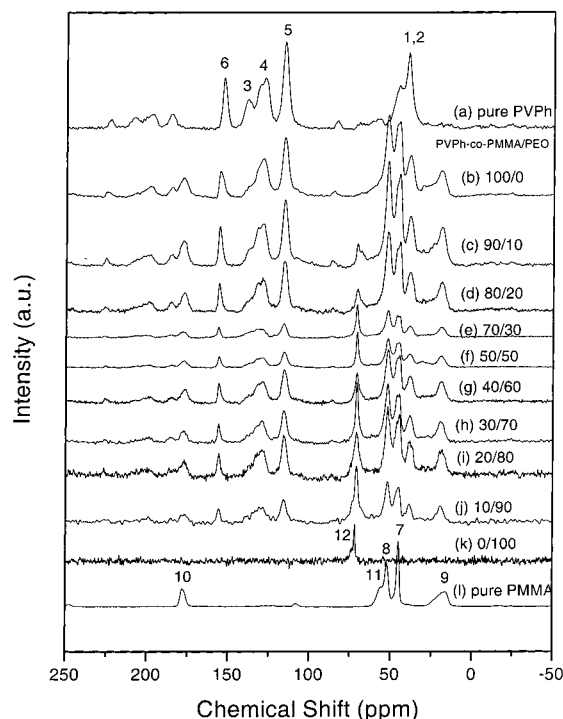
Figure 9. [13]C CPMAS spectra at room temperature for pure PVPh, pure PMMA and various PVPh-*co*-PMMA/PEO blends: (a) pure PVPh; (b) 100/0; (c) 90/10; (d) 80/20; (e) 70/30; (f) 50/50; (g) 40/60; (h) 30/70; (i) 20/50; (j) 10/90; (k) 0/100; (l) pure PMMA.

Table 4. Chemical Shift of the ^{13}C CP/MAS Spectra of PEO, PVPh, PMMA, and Their Blends

blend composition	C-6	C-10	C-12
pure PMMA		177.00	
pure PVPh	153.24		
PVPh-*co*-PMMA/PEO			
100/0	155.61	178.33	
90/10	155.76	178.18	70.72
80/20	156.15	178.12	70.71
70/30	156.19	178.07	70.93
50/50	156.20	177.11	70.79
40/60	156.22	177.09	70.93
30/70	155.96	177.05	70.79
20/80	155.79	177.00	71.02
10/90	155.78	176.55	70.88
0/100			71.76

tallization is retarded and even inhibited by adding the amorphous PVPh-*co*-PMMA polymer.

Solid State NMR Analyses. Solid-state NMR spectroscopy provides further insight into the phase behavior and morphology of polymer blends involving hydrogen bond formation. Figure 9 shows the ^{13}C CPMAS spectra of pure PVPh, PMMA, PVPh-*co*-PMMA, PEO, and PVPh-*co*-PMMA/PEO blends of various compositions. The pure PVPh has six resonance peaks and the hydroxyl-substituted carbon in the phenolic ring (C-6) is at 153.2 ppm. Five peaks can be observed for pure PMMA and the resonance peak at 177.0 ppm is from the carbonyl carbon (C-10). The pure PEO should have two bands corresponding to the methylene carbons (C-12)[27] in the crystalline phase at 72 ppm and the amorphous phase at 70 ppm. All other peak assignments are assigned in Figure 9 as shown in Figure 1. Peak positions of these three resonance peaks for the pure components and blends are listed in Table 4. The variation in the observed chemical shift (1.33 ppm) of the carbonyl carbon (C=O) between the pure PVPh-*co*-
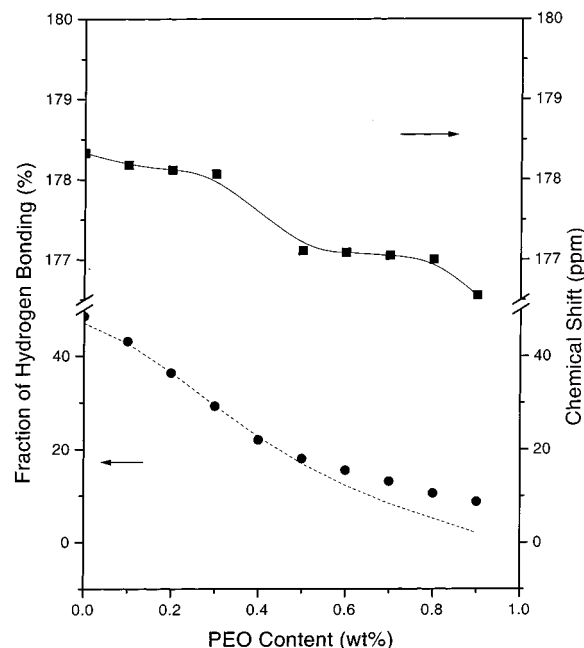

Figure 10. Chemical shift and fraction of hydrogen bonding of carbonyl groups vs PEO content.

PMMA and the pure PMMA indicates the existence of a specific interaction between the PVPh and PMMA segments. It is well-known that the hydrogen bonding in polymer blends can affect the chemical environment of the neighboring molecules, causing a chemical downfield shift. Figure 10 shows the fraction of hydrogen bonding of the carbonyl (Table 2) in FTIR and the corresponding chemical shift in solid state NMR spectra at room temperature vs PEO content. The chemical shift and the fraction of hydrogen bonding of the carbonyl exhibit the same decreasing trend as PEO content increases. Evidently, the strength of the hydroxyl–ether interassociation exceeds that of the hydroxyl–carbonyl self-association. The dashed line is the predicted fraction of hydrogen-bonded carbonyl groups at room temperature according to the Painter–Coleman association model. The theoretical curve accurately predicts the observed hydrogen-bonded carbonyl content at low PEO contents, but deviation increases, due to the intramolecular screening effect[28] and the presence of a crystalline phase as PEO content in the blend increases.

The hydroxyl-substituted carbon in the phenolic ring (C-6) of pure PVPh-*co*-PMMA is at 155.61 ppm. Compared with the pure PVPh at 153.24 ppm, a downfield shift of 2.37 ppm is observed, implying strong intramolecular self-association between PVPh and PMMA segments in the pure PVPh-*co*-PMMA copolymer. Figure 11 shows the solid-state NMR chemical shift and the FTIR wavenumbers of the hydroxyl group against the PEO content. The chemical shift increases as PEO content increases up to a maximum of 156.25 ppm for the blend containing 60 wt % PEO and then decreases gradually as the PEO content increases further. The FTIR wavenumber decreases with increasing PEO content and approaches a minimum at 3350 cm^{−1}, also for the blend containing 60 wt % PEO, and then increases with further increase of the PEO content. It is well-known that a downfield chemical shift (higher chemical shift) in solid-state NMR and the wavenumber shift to lower wavenumber in FTIR both indicate stronger specific interactions between components. Therefore, the solid-state NMR and FTIR results show the
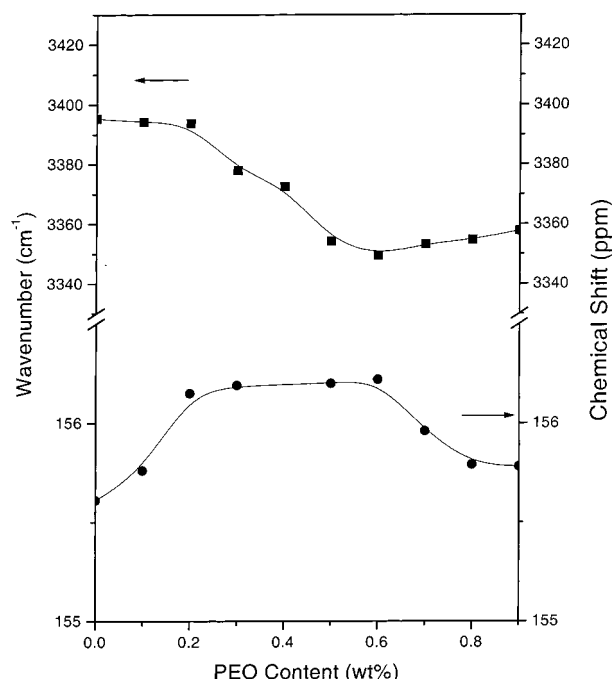
Figure 11. Chemical shift and wavenumber of the hydroxyl groups at room temperature vs PEO content.

Figure 12. FTIR spectra recorded at 150 °C at 2700 cm^{-1}-4000 cm^{-1} region for various PVPh-*co*-PMMA/PEO blends: (a) 100/0; (b) 90/10; (c) 80/20; (d) 70/30; (e) 60/40; (f) 50/50; (g) 40/60; (h) 30/70; (i) 20/50; (j) 10/90.

Table 5. $T_{1\rho}{}^{H}$ Values of Pure PVPh and Various PVPh-*co*-PMMA/PEO Blend Compositions

blend composition	115 ppm	70 ppm	
pure PVPh	7.24		
PVPh-*co*-PMMA/PEO			
100/0	12.08		
80/20	5.12	1.48	
40/60	4.30	1.38	
20/80	4.77	0.95	3.93
0/100		0.08	7.84

same trends over the entire compositions. The lower chemical shift and higher wavenumber at higher PEO content can be explained by the fact that these blend systems possess a crystalline phase. Consequently, the hydroxyl–ether interassociation tends to decrease between the PVPh and PEO segment due to reduced chain mobility in the PEO crystalline phase.

IR spectra for these blends were measured at 150 °C to support this claim. Measurements carried out at this temperature, above the melting and glass transition temperatures, can eliminate the effect from the PEO crystallization. Therefore, the equilibrium condition is reasonably attained at this temperature. Figure 12 shows the hydroxyl-stretching absorption region of the pure PVPh-*co*-PMMA and various PVPh-*co*-PMMA/PEO blends between 2700 and 4000 cm^{-1}. The wavenumber decreases with increasing PEO content for the entire composition range. This result supports the claim that the previous observed higher wavenumber and lower chemical shift of blends containing higher PEO content (Figure 11) are indeed caused by the presence of the PEO crystalline phase with relatively lower chain mobility. We will discuss the chain mobility by spin lattice relaxation time in the rotating frame using solid-state NMR in the next section.

Proton Spin Lattice Relaxation Time in the Rotating Frame Analyses. The spin lattice relaxation time in the rotating frame ($T_{1\rho}{}^{H}$) was measured to examine the homogeneity of PVPh-*co*-PMMA blends on the molecular scale. The magnetization of resonance is expected to decay according to the following exponential function model given by eq 6, according to the spin locking mode employed in this study, where $T_{1\rho}{}^{H}$ is the

$$M_\tau = M_0 \exp\lfloor -\tau/T_{1\rho}(H)\rfloor \qquad (6)$$

spin lattice relaxation time in the rotating frame. τ is the delay time used in the experiment and M_τ is the corresponding resonance. $T_{1\rho}{}^{H}$ can be obtained from the slope of $\ln(M_\tau/M_0)$ vs τ,
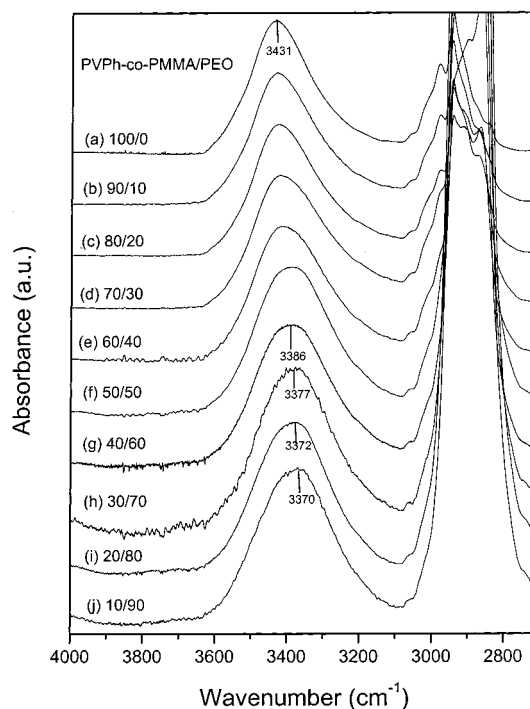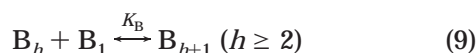
Table 5 summarizes those $T_{1\rho}{}^{H}$ values derived from the binary exponential analysis, indicating that the blend with high PVPh-*co*-PMMA content exhibits single exponential. However, the biexponential decay gradually appears at higher PEO contents at 70 ppm. A semicrystalline polymer will have two proton spin lattice relaxations; the crystalline phase and the amorphous phase, attributed to the long and short relaxation components, respectively. According to Table 5, the amorphous $T_{1\rho}{}^{H}$ decreases with increasing PEO content in the blend. Meanwhile, a high $T_{1\rho}{}^{H}$ value for PVPh-*co*-PMMA/PEO = 80/20 blend, implies that the polymer mobility is retarded reflecting the more rigid character of the PVPh-*co*-PMMA. To the contrary, a decrease of the $T_{1\rho}{}^{H}$ value in the PEO rich region is associated with increased mobility of the amorphous PEO, related to the reduction of the intermolecular hydrogen bonding strength. An increasing amount of the long relaxation component with increasing PEO suggests the existence of a more crystalline PEO phase in the blend.

Table 5 also shows that both pure PVPh and PVPh-*co*-PMMA/PEO blends exhibit only single-exponential relaxation throughout all blends at 115 ppm, indicating good miscibility and dynamic homogeneity in the PVPh-*co*-PMMA phase. The maximum diffusive path length L can be estimated using the approximate eq 7.[29−31] For $T_{1\rho}{}^{H}$ of 5 ms and a effective spin diffusion coefficient,

$$L = (6DT)^{1/2} \tag{7}$$

D, of 10^{-16} m^2 s^{-1}, the dimensions of these PVPh-*co*-PMMA/PEO blends are below 2−3 nm in the amorphous phase. Interestingly, the $T_{1\rho}{}^{H}$ has a minimum value for the PVPh-*co*-PMMA = 40/60 blend showing that the overall chain mobility is maximal at this composition. This observation agrees with the earlier result concerning hydroxyl group association obtained by FTIR and solid-state NMR. In addition, all blends show shorter $T_{1\rho}{}^{H}$ than that of the pure PVPh-*co*-PMMA implying that the PVPh-*co*-PMMA mobility also increases with the increase of PEO content.

Stoichiometric Equations by Painter-Coleman Association Model. In our previous study,[32,33] we adopted the Painter−Coleman association model (PCAM) to predict thermodynamic properties. However, all the blends investigated in this study contain a self-associating polymer B and a nonself-associating polymer A, which can interact with B. This PCAM model has been modified to account for not only self-association equilibrium in B but several other self-association equilibria, all of which can be studied for the blends in this study.[34,35] According to the PCAM model, we designate B, C, and A as vinylphenol, methyl methacrylate, and ethylene oxide units, respectively, and K_2, K_B, K_C, and K_A as their corresponding association equilibrium constants.

$$B_1 + B_1 \overset{K_2}{\rightleftharpoons} B_2 \tag{8}$$

$$B_h + B_1 \overset{K_B}{\rightleftharpoons} B_{h+1} \; (h \geq 2) \tag{9}$$

$$B_h + C_1 \overset{K_C}{\rightleftharpoons} B_h C \tag{10}$$

$$B_h + A_1 \overset{K_A}{\rightleftharpoons} B_h A \tag{11}$$

These four equilibrium constants can be expressed as follows in terms of volume fractions

$$\Phi_B = \Phi_{B1} \Gamma_2 \left[1 + \frac{K_A \Phi_{A1}}{r_A} + \frac{K_C \Phi_{C1}}{r_C} \right] \tag{12}$$

$$\Phi_A = \Phi_{A1}[1 + K_A \Phi_{B1} \Gamma_1] \tag{13}$$

$$\Phi_C = \Phi_{C1}[1 + K_C \Phi_{B1} \Gamma_1] \tag{14}$$

where

$$\Gamma_1 = \left(1 - \frac{K_2}{K_B} \right) + \frac{K_2}{K_B} \left(\frac{1}{(1 - K_B \Phi_{B1})} \right) \tag{15}$$

$$\Gamma_2 = \left(1 - \frac{K_2}{K_B} \right) + \frac{K_2}{K_B} \left(\frac{1}{(1 - K_B \Phi_{B1})^2} \right) \tag{16}$$

Φ_B, Φ_A, and Φ_C are the volume fractions of repeat units in the blend, Φ_{B1}, Φ_{A1}, and Φ_{C1} are the volume fractions of isolated units in the blend and $r_A = V_A/V_B$ and $r_C = V_C/V_B$ are the ratios of segmental molar volumes.

The self-association values of PVPh ($K_2 = 21.0$ and $K_B = 66.8$), the self-association between PVPh and PMMA ($K_C = 67.4$) and interassociation between PVPh and PEO ($K_A = 88.3$) were determined by Coleman et al.[36,37] We did not adopt the interassociation equilibrium ($K_C = 37.5$) between pure PVPh and pure PMMA blend

Table 6. Curve-Fitting Results of PVPh-*co*-PMMA/PEO = 60/40 Blend at Various Temperatures

	free C=O			H-bonded C=O			
temp (°C)	ν (cm^{-1})	$W_{1/2}$ (cm^{-1})	A_f (%)	ν (cm^{-1})	$W_{1/2}$ (cm^{-1})	A_b (%)	fb (%)
25	1728.3	18.71	74.38	1703.7	22.12	25.62	18.66
50	1728.5	19.23	74.54	1703.0	22.46	24.46	18.54
80	1728.8	19.33	73.56	1703.4	23.18	26.44	19.33
100	1728.9	19.32	72.61	1703.9	23.43	27.39	20.09
120	1729.2	19.06	70.19	1704.8	24.15	29.81	22.06
140	1729.4	19.32	69.34	1705.0	23.82	30.66	22.76
150	1729.6	19.37	68.20	1705.5	24.54	31.80	23.71
160	1729.7	19.42	67.45	1705.8	25.02	32.55	24.33
170	1729.7	19.56	66.93	1706.1	25.55	33.07	24.77

derived by Cesteros et al.[38] due to the composition heterogeneities in the hydrogen bonding polymer system.[36] Therefore, we used the equilibrium constant previously reported by Coleman et al. for poly(vinylphenol-*co*-ethyl methacrylate) ($K_C = 67.4$). Table 3 presents the corresponding values of the equilibrium constants and segmental molar volumes. The fraction of hydrogen bonding for a given blend composition can be calculated from eqs 11−13, using

$$f_{HB} = 1 - \frac{\Phi_{C1}}{\Phi_C} \tag{17}$$

Therefore, the predicted fraction of hydrogen bonding of carbonyl groups (dashed line) in Figure 11 can be calculated numerically.

FTIR Analyses at Various Temperatures. Table 6 summarizes the quantitative analysis of the fraction of the hydrogen bonding carbonyl groups from 25 to 170 °C for the PVPh-*co*-PMMA/PEO = 40/60 blend which decreases from 25 to 50 °C, and then increase with further increases of temperature. In general, the $f_{HB}{}^{C=O}$ decreases with increasing temperature as would be expected. Initially, this observation seems counterintuitive. However, for a multicomponent hydrogen-bonding system containing different competing acceptor groups, different enthalpies from different hydrogen bond formations can markedly affect the equilibrium constant. The same phenomenon is observed in poly-(vinylphenol-*co*-*n*-butyl methacrylate) and the styrene-*stat*-2-vinylpyridine blend system observed by Coleman et al.[39]

From the Van't Hoff relationship shown in eq 18, we

$$K = -\frac{\Delta h}{RT} + C \tag{18}$$

can plot the values of the different equilibrium constants as a function temperature from 25 to 200 °C, as shown in Figure 13. Curves K_A and K_C represents the competition of the hydroxyl−ether interassociation and hydroxyl−carbonyl self-association, respectively. The equilibrium constants, K_A and K_C change with temperature at different rates. It can be found that $K_A = K_C$ at about 70 °C. This result implies that the equivalent numbers of the hydroxyl−carbonyl association are favored because K_C exceeds K_A above 70 °C. Therefore, the observation that the fraction of hydrogen bonded carbonyl groups increases with increasing temperature can be explained by the Painter−Coleman association model.

Conclusions

PVPh-*co*-PMMA and PEO are completely miscible in an amorphous phase over the entire composition range.
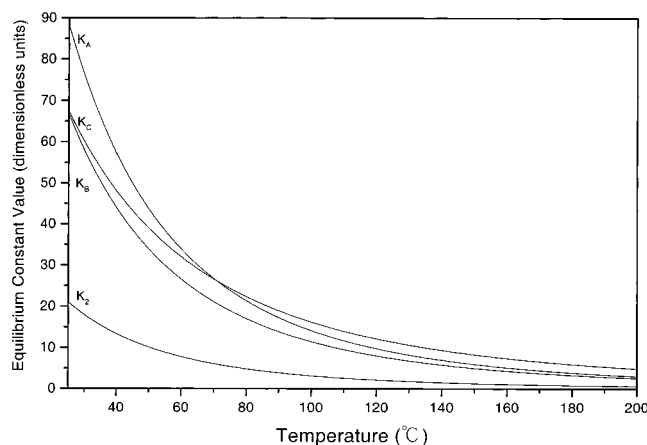
Figure 13. Equilibrium constant values as a function of temperature from 25 to 200 °C.

A negative polymer−polymer interaction energy density *B* was calculated from the melting depression of PEO, using the Nishi−Wang equation and the single-exponential decay of proton spin−lattice relaxation times in the rotating frame ($T_{1\rho}{}^{H}$) in amphorous PVPh-*co*-PMMA phase, as can be observed with solid state NMR. The Kwei equation can accurately predict T_gs from experimental results due to the existence of hydrogen bonding between PVPh-*co*-PMMA and PEO.

Both ¹³C solid-state NMR and FTIR were employed to study the specific interaction at various compositions and various inter and intramolecular hydrogen bonding. The hydroxyl−ether association dominates at room temperature but the hydroxyl−carbonyl association dominates at higher temperatures (>70 °C). The Painter−Coleman association model (PCAM) is able to predict three interacting functional groups according to our experimental results at various temperatures.

References and Notes

(1) Miyoshi, T.; Takegoshi, K.; Hikichi, K. *Polymer* **1996**, *37*, 11.
(2) Chu, P. P.; Wu, H. D. *Polymer* **2000**, *41*, 101.
(3) Brus, J.; Dybal, J.; Schmidt, P.; Kratochvil, J.; Baldrain, J. *Macromolecules* **2000**, *33*, 6448.
(4) Lezcano, E. G.; Coll, C. S.; Prolongo, M. G. *Polymer* **1996**, *37*, 3603.
(5) Li, D.; Brisson, J. *Macromolecules* **1996**, *29*, 868.
(6) Chen, H. L.; Liu, H. H.; Lin, J. S. *Macromolecules* **2000**, *33*, 4856.
(7) Sawatari, C.; Kondo, T. *Macromolecules* **1999**, *32*, 1949.
(8) Wang, J.; Cheung, M. K.; Mi, Y. *Polymer* **2001**, *42*, 2077.
(9) Hill, D. J. T.; Whittaker, A. K.; Wong, K. W. *Macromolecules* **1999**, *32*, 5285.
(10) Zhong, Z.; Guo, Qipeng.; Mi, Y. *Polymer* **1998**, *40*, 27.
(11) Zhang, X.; Takegoshi, K.; Hikichi, K. *Macromolecules* **1991**, *24*, 5756.
(12) Cheung, M. K.; Wang, J.; Zheng, S.; Mi, Y. *Polymer* **2000**, *41*, 1469.
(13) Kesel, C. D.; Lefevre, C.; Nagy, J. B.; David, C. *Polymer* **1999**, *40*, 1969.
(14) Etxeberria, A.; Guezala, S.; Iruin, J. J.; Campa, J. G.; Abajo, J. D. *Polymer* **1998**, *39*, 1035.
(15) Mekhilef, N.; Hadjiandreou, P. *Polymer* **1995**, *36*, 2165.
(16) Qin, C.; Pires, A. T. N.; Belfiore, L. A. *Macromolecules* **1991**, *24*, 666.
(17) Coleman, M. M.; Yang, X.; Painter, P. C.; Graf, J. F. *Macromolecules* **1992**, *25*, 4414.
(18) Coleman, M. M.; Graf, J. F.; Painter, P. C. *Specific Interactions and the Miscibility of Polymer Blends*; Technomic Publishing: Lancaster, PA, 1991.
(19) Fox T. G. *J. Appl. Bull. Am. Phys. Soc.* **1956**, *1*, 123.
(20) Gordon, M.; Taylor, J. S. *J. Appl. Chem.* **1952**, *2*, 493.
(21) Kwei, T. J. *Polym. Sci.: Polym. Lett. Ed.* **1984**, *22*, 307.
(22) Nishi, T.; Wang, T. T. *Macromolecules* **1975**, *8*, 909.
(23) Flory, P. J. *Principles of Polymer Chemistry*; Cornell University Press: Ithaca, NY, 1953.
(24) Hoffman, J. D.; Weeks, J. J. *J. Chem. Phys.* **1965**, *42*, 4301.
(25) Jo, W. H.; Lee, S. C. *Macromolecules* **1990**, *23*, 2261.
(26) Chintapalli, S.; Frech, R. *Macromolecules* **1996**, *29*, 3499.
(27) Schilling, F. C.; Tonelli, A. E.; Cholli, A. L. *J. Polym. Sci. Polym.; Phys. Ed.* **1992**, *30*, 91.
(28) Painter, P. C.; Veytsman, B.; Kumar, S.; Graf, J. F.; Xu, Y.; Coleman, M. M. *Macromolecules* **1997**, *30*, 932.
(29) McBrierty, V. J.; Douglass, D. C. *J. Polym. Sci., Macromol. Rev.* **1981**, *16*, 295.
(30) Demco, D. E.; Johansson, A.; Tegenfeldt, *J. Solid State Nucl. Magn. Reson.* **1995**, *4*, 13.
(31) Clauss, J.; Schmidt-Rohr, K, W. H. *Acta Polym.* **1993**, *44*, 1.
(32) Kuo, S. W.; Chang, F. C. Maunuscript submitted for publication.
(33) Wu, H. D.; Chu, P. P.; Ma, C. C. M.; Chang, F. C. *Macromolecules* **1999**, *32*, 3097.
(34) Menestrel, C. L.; Bhagwagar, D. E.; Painter, P. C.; Coleman, M. M.; Graf, J. F. *Macromolecules* **1992**, *25*, 7101.
(35) Cesteros, L. C.; Isasi, J. R.; Katime, I. *Macromolecules* **1993**, *26*, 7256.
(36) Coleman, M. M.; Xu, Y.; Painter, P. C. *Macromolecules* **1994**, *27*, 127.
(37) Serman, C. J.; Xu, Y.; Painter, P. C.; Coleman, M. M. *Polymer* **1991**, *32*, 516.
(38) Serman, C. J.; Painter, P. C.; Coleman, M. M. *Polymer* **1991**, *32*, 1049.
(39) Coleman, M. M.; Narvett, L. A.; Painter, P. C. *Polymer* **1998**, *39*, 5867.

MA010047K